

Non-linear dynamics and inner-ring photoluminescence pattern of indirect excitons

Mathieu Alloing¹, Aristide Lemaître², Elisabeth Galopin² and François Dubin¹

¹ *ICFO-The Institut of Photonic Sciences, Av. Carl Friedrich Gauss,
num. 3, 08860 Castelldefels (Barcelona), Spain and*

² *Laboratoire de Photonique et Nanostructures, LPN/CNRS, Route de Nozay, 91460 Marcoussis, France*

(Dated: November 14, 2018)

We study the photoluminescence dynamics of ultra-cold indirect excitons optically created in a double quantum well heterostructure. Above a threshold laser excitation, our experiments reveal the apparition of the so-called inner photoluminescence ring. It is characterized by a ring shaped photoluminescence which suddenly collapses once the laser excitation is terminated. We show that the spectrally resolved dynamics is in agreement with an excitonic origin for the inner-ring which is formed due to a local heating of indirect excitons by the laser excitation. To confirm this interpretation and exclude the ionization of indirect excitons, we evaluate the excitonic density that is extracted from the energy of the photoluminescence emission. It is shown that optically injected carriers play a crucial role in that context as these are trapped in our field-effect device and then vary the electrostatic potential controlling the confinement of indirect excitons. This disruptive effect blurs the estimation of the exciton concentration. However, it is suppressed by smoothing the electrostatic environment of the double quantum well by placing the latter behind a super-lattice. In this improved geometry, we then estimate that the exciton density remains one order of magnitude smaller than the critical density for the ionization of indirect excitons (or Mott transition) in the regime where the inner-ring is formed.

PACS numbers: 78.67.De, 73.63.Hs, 73.21.Fg, 78.47.jd

I. INTRODUCTION

In the quest for a model system to study ultra-cold dipolar gases in the solid-state, semiconductor heterostructures offer a very promising route. In particular, a field-effect device embedding a double quantum well (DQW) opens a unique opportunity to engineer and control the so-called spatially indirect excitons. These dipolar quasi-particles result from the Coulomb attraction between electrons and holes that are spatially separated and confined in distinct quantum wells. This situation is achieved by applying an external electric field perpendicularly to a DQW such that the minimum energy states for electrons and holes lie in distinct quantum wells. First, the spatial separation imposed between electronic carriers provide indirect excitons with a large electric dipole, aligned perpendicularly to the plane of the DQW, such that repulsive dipolar interactions between excitons are dominant at low temperature. Remarkably, the dipolar repulsions yield a screening of the disorder of the semiconductor matrix [1, 2] and also trigger a rapid expansion of exciton gases [3]. In addition, spatially separating electrons and holes highly reduces the overlap between the electronic wave-functions. Thus, indirect excitons of double quantum wells exhibit radiative lifetimes orders of magnitude longer than in single quantum wells. At the same time, they benefit from an efficient thermalization by the semiconductor lattice bringing dense gases into the sub-Kelvin temperature regime [4, 5].

In general, indirect excitons can be electrically or optically created in double quantum wells. In the latter case, micro-photoluminescence experiments have revealed that indirect excitons form characteristic spatial patterns and particularly ring-shaped structures. Pre-

cisely, above a threshold laser excitation a wide (outer) luminescence ring is observed hundreds of microns away the excitation spot and where electronic carriers are created [6, 7]. In addition, a narrow (inner) luminescence ring is formed around the excitation spot itself [6, 8–10]. On the one hand, it has been established that the outer-ring signals the recombination between optically and electrically injected carriers [11, 12]. On the other hand, the origin of the inner photoluminescence ring has first been attributed to a laser induced heating of indirect excitons: combined experimental and theoretical studies have shown that the inner luminescence ring is the signature of the transport and subsequent cooling of the indirect excitons outside the excitation spot [8, 10, 13]. Alternatively, the apparition of the inner ring has been discussed in terms of the ionization of indirect excitons by experiments which have underlined that it is formed at the onset of the Mott transition [9]. Consequently, the exciton concentration shall be accurately estimated in the regime where the inner ring appears. However, we show here that this can constitute a delicate task since the exciton density is deduced from the energy shift of the photoluminescence emission which depends on the field-effect device embedding the DQW, and particularly on stray electric fields or charges that may be optically/electrically injected.

Here, we report experiments probing the dynamics of the photoluminescence emission of indirect excitons in the regime where the inner photoluminescence ring is formed. Our experiments are carried out with high spatial, spectral and temporal resolutions at a bath temperature of 400 mK. Thus, the main characteristics of the inner-ring are revealed. Within the region that is laser excited, these characteristics include a non-linear

dynamics marked by a jump of the photoluminescence signal at the end of the laser pulse together with a rapid decrease of the emitted spectral linewidth. On the other hand, the photoluminescence emitted outside of the illuminated region exhibits a reduced photoluminescence jump and is also spectrally narrower, even during laser excitation. These observations are in good agreement with the works of Butov and coworkers [8, 10, 13] and suggest for our experiments that the inner ring marks the recombination of indirect excitons heated locally by the laser excitation. To confirm this interpretation, we analyzed the energy shift of the photoluminescence emission in order to quantify the exciton density in the regime where the inner-ring is formed. Thus, we show that a fraction of photo-injected carriers is trapped in our field-effect device, at the Schottky barrier between our metallic gate electrode and the semiconductor heterostructure. Accordingly, the internal electric field is varied by the photo-excitation so that the photoluminescence exhibits very large energy shifts preventing a quantitative estimation of the exciton density. In this context, we report studies of a second device where the DQW is placed behind a super-lattice where carriers can be optically injected and confined. The super-lattice is used to screen fluctuations of the potential at the gate electrode. For this second device, our experiments show that the DQW heterostructure is then subject to an homogeneous electric field as the laser excitation is varied, i.e. as the concentration of photo-injected carriers is increased. In this improved situation, we estimate that the exciton density remains about an order of magnitude below the predicted onset for the Mott transition in the regime where the inner ring arises. This allows us to conclude for our experiments that the apparition of the inner-ring marks the recombination of indirect excitons.

II. EXPERIMENTAL APPARATUS AND FIELD-EFFECT DEVICE

We present in Figure 1 the first field-effect device that we studied experimentally. It is made of a *metal-in* heterostructure where a DQW constituted by two 8 nm wide GaAs quantum wells separated by a 4 nm $\text{Al}_{0.33}\text{Ga}_{0.67}\text{As}$ barrier is placed in a $\text{Al}_{0.33}\text{Ga}_{0.67}\text{As}$ layer with a thickness equal to 1 μm . The DQW is positioned 50 nm above a Si-doped GaAs buffer ($n_{\text{Si}} \sim 10^{18} \text{ cm}^{-3}$) acting as the electrical back-gate, grounded in our experiments. On the surface of the sample, a 100 μm wide disk shape semi-transparent electrode (Au/Ti, 4/4 nm thick) has been deposited and is biased at V_g to control the electric field inside the field-effect device. Thus, our device implements a 100 μm wide electrostatic trap for indirect excitons (see Fig. 1.d.) where the minimum energy states for electrons and holes lie in separate quantum wells. In the following, a positive bias is applied to the top gate electrode such that electrons and holes are confined in the top and bottom quantum wells respectively (see Fig. 1.c). Finally,

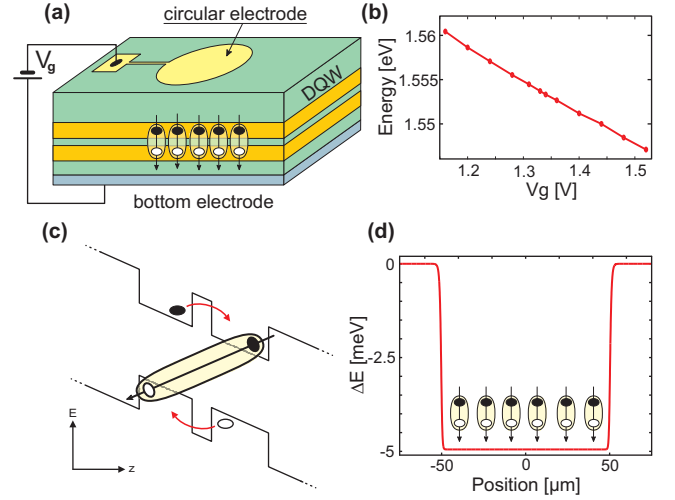


FIG. 1. (Color Online) (a): Schematic representation of the field-effect device. Electrons and holes are displayed by filled and open circles respectively. (b): Energy of the photoluminescence emission of indirect excitons as a function of the gate voltage V_g . (c) Band diagram of the DQW along the vertical direction z . (d) Trapping potential $\Delta E = d_z \cdot E_z$ created by the circular electrode for an effective applied voltage $V_g - V_s = 0.4 \text{ V}$.

let us note that we probe a device where the DQW is placed close to the back-gate electrode. This geometry is promising to engineer opto-electronic devices by reducing the surface electrodes dimensions to few micrometers while an homogeneous electric field is maintained at the position of the double quantum well [14–17].

In the experiments presented in the following, we placed the semiconductor sample on the Helium 3 insert of a closed cycle Helium 4 cryostat (Heliox-ACV from Oxford Instruments). An aspheric lens with a 0.6 numerical aperture is embedded inside the cryostat in front of the sample and positioned by piezo-electric transducers (ML17 from MechOnics-Ag). We optimized the optical resolution of our microscope by introducing a mechanical coupling between the Helium 3 insert and the part holding the aspheric lens. Thus, the amplitude of mechanical vibrations does not exceed 2 microns (in a frequency range up to $\sim 1 \text{ KHz}$) while the sample can be cooled to temperatures as low as 350 mK. For the following experiments, indirect excitons were optically created in the electrostatic trap by a laser excitation at 640 nm. The incident photon energy was then greater than the band gap of the GaAs layers while indirect excitons are only formed following the energy relaxation of electrons and holes in the DQW. To study the dynamics of optically created indirect excitons we utilized a transient laser excitation with 50 ns long laser pulses at a repetition rate of 2 MHz. The laser light was focused at the center of the electrostatic trap and had a Gaussian profile with a full width at half maximum of $\approx 7(1) \mu\text{m}$. The photoluminescence emitted by the sample was collected by the aspheric lens used for photoexcitation and directed to

an imaging spectrometer coupled to an intensified CCD camera (Picostar-UF from La Vision). Thus, we studied the dynamics of indirect excitons with a 2 ns time resolution, either in real space or including a spectral resolution of 200 μeV .

First, we studied the opto-electronics characteristics of our device by analyzing the photoluminescence spectrum under low laser excitation and as a function of the gate voltage, V_g . We then identified the following regimes: For $V_g \leq V_s = 1(0.05)\text{V}$, the energy of the direct excitons recombination does not vary and the photoluminescence of spatially indirect excitons is absent from the spectrum. This behavior signals that a Schottky barrier with an amplitude V_s is formed in our device at the interface between the semitransparent metallic contact and the semiconductor heterostructure. The Schottky barrier results from both the rectification of potentials at the contact and from surface states that act as impurity levels distributed in the semiconductor forbidden gap [18, 19]. Thus, for $V_g \leq V_s$, the potential applied to the semitransparent electrode mostly drops across the Schottky barrier and the DQW remains effectively unpolarized. Note that our field-effect device exhibits a built-in potential V_s that is comparable to its theoretical expectation [18] and to what reported with similar structures [20]. On the other hand, for $V_g \geq V_s$, the photoluminescence of direct excitons initially shifts to lower energies before vanishing while the emission of charged excitons appears in the spectrum. This indicates that free carriers are trapped in the DQW, though we observe a photo-current of ≤ 100 nA which is a rather typical value. At the same time, the emission of indirect excitons arises and is marked by its energy that varies linearly with increasing V_g (see Fig. 1.b). This behavior reveals the quantum confined Stark effect, i.e. the interaction between the electric dipole \vec{d} of indirect excitons and the electric field applied in the heterostructure \vec{E} , which varies as $-\vec{d} \cdot \vec{E}$. For our sample design the in-plane components of \vec{E} can be neglected leading to a confinement of the indirect excitons under the electrode with a theoretical amplitude for the trapping potential $\Delta E = d_z \cdot E_z \sim 5$ meV for an effective applied bias $V_g - V_s = 0.4$ V (see Fig. 1.d.).

III. EXPERIMENTAL RESULTS

We present in Figure 2 the central result of our work, namely the apparition of a ring shaped photoluminescence above a threshold excitation of $\sim 1.8 \text{ W.cm}^{-2}$ [21]. Remarkably, this emission profile is solely observed during the laser excitation and the ring collapses 4 ns after the laser pulse is terminated. As mentioned above, experimental studies have previously reported the apparition of this pattern that is referred to as inner-ring [6, 8–10]. To determine the mechanisms responsible for the formation of the inner-ring in our experiments, we analyzed spatially and spectrally the photoluminescence. Therefore, we selected the center of the inner-ring pattern along

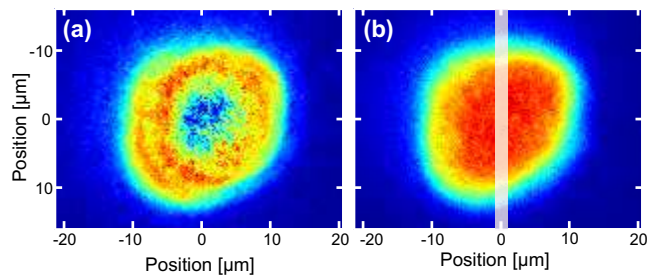


FIG. 2. (Color Online) Real image of the photoluminescence emission of indirect excitons at the end of the laser excitation (a) and 6 ns later (b). The semi-transparent white region indicates the position of the entrance slit of the imaging spectrometer. The experiments were realized at a bath temperature $T_b = 400$ mK and for a laser excitation power $P_{ex} = 14.8 \text{ W.cm}^{-2}$.

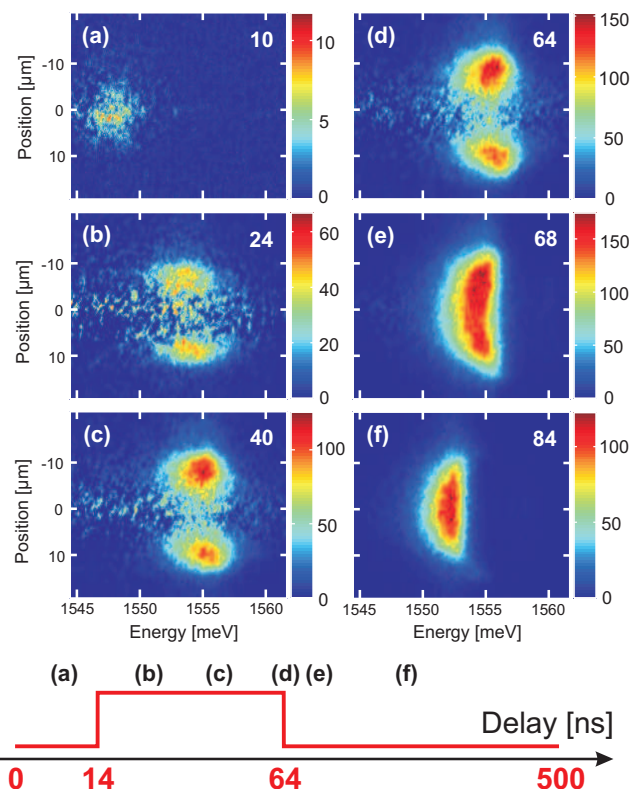


FIG. 3. (Color Online) (a)-(f): Spatially resolved emission spectrum for $P_{ex} = 14.8 \text{ W.cm}^{-2}$ recorded in 2 ns intervals at various time delays. The corresponding time delays are indicated in each image and reminded on a schematic of the laser pulse. The intensity is colored-scaled independently for each spectrum. Experimental results were obtained at $T_b = 400$ mK.

the vertical direction (this region is marked by the semi-transparent rectangle in Figure 2 and matches the entrance slit of our imaging spectrograph) and spectrally dispersed this component to study the dynamics of the inner-ring in the real-frequency space.

In Figure 3, the spectrally resolved photoluminescence

along the vertical direction at the center of the ring pattern is presented. Precisely, a sequence of images taken during and following the 50 ns long laser pulse is displayed. For each image, the vertical direction marks the spatial coordinate and the horizontal axis the energy. First, we note in Figure 3 that the inner-ring is rapidly formed, within the first 10 ns of the laser pulse. Furthermore, the emission spectrally broadens during the laser excitation and reaches at the end of the laser pulse a width of ~ 5.2 meV in the darker part (which corresponds to the laser excited region) and ~ 4 meV for the “up” and “down” bright spots (see also Fig. 4.b). To examine the nature of the emission at the end of the laser excitation, let us compare the spectral widths to that emitted by an unbound electron hole plasma. The latter value is deduced by first estimating the density, n_M , at which the Mott transition occurs. It is controlled by the Bohr radius of indirect excitons, a_B ($n_M \sim (1/a_B)^2$), and for our DQW we have $a_B \approx 20$ nm such that $n_M \approx 2 \cdot 10^{11} \text{ cm}^{-2}$. Thus, the minimum spectral width emitted by an electron-hole plasma reads $\Gamma_{e-h}^{(min)} \sim \pi \hbar^2 n_M (1/m_e + 1/m_h)$, where m_e and m_h denote the electron and hole effective mass respectively, and we deduce $\Gamma_{e-h}^{(min)} \geq 5$ meV for our experiments. The latter value is somewhat comparable to the spectral width of the photoluminescence emitted at the center and along the perimeter of the inner-ring. Thus, analyzing the photoluminescence spectral width does not provide an unambiguous determination of the nature of the emission. To establish whether the spectrally broad emission marks a significant ionization of excitons, we now discuss the dynamics of the photoluminescence once the laser excitation is switched off.

As illustrated in Figures 2 and 3.e-f, the inner-ring has a distinctive dynamics and collapses in a time interval as short as few nanoseconds after the falling edge of the laser pulse. This transition is marked by two coincident phenomena in the central region of the inner-ring: a sudden enhancement of the photoluminescence signal (or PL-jump) and a rapid decrease of the photoluminescence spectral width. These aspects are illustrated in Figure 4 which displays the dynamics of the emission at the center and at two other spatial positions, as depicted in the inset of Fig. 4.b. We first note in Fig. 4.a that at the center of the inner-ring the PL-jump has a far larger amplitude (up to ~ 2.5) than along the bright region of the ring pattern where it reaches 1.2 [22]. In fact, we note that the spatial variation of the PL-jump reproduces the profile of the laser excitation, as shown in Fig. 4.c. These observations well agree with the works of Butov and co-workers and then with hydrodynamical calculations predicting that the inner ring is formed due to the heating of indirect excitons induced by the laser excitation [5, 8, 10, 13]: The PL-jump marks a sharp increase of the population of the optically active lowest energy states after the laser excitation, i.e. the rapid thermalization of the corresponding “hot” indirect excitons. On the other hand, along the circumference of the inner-ring indirect

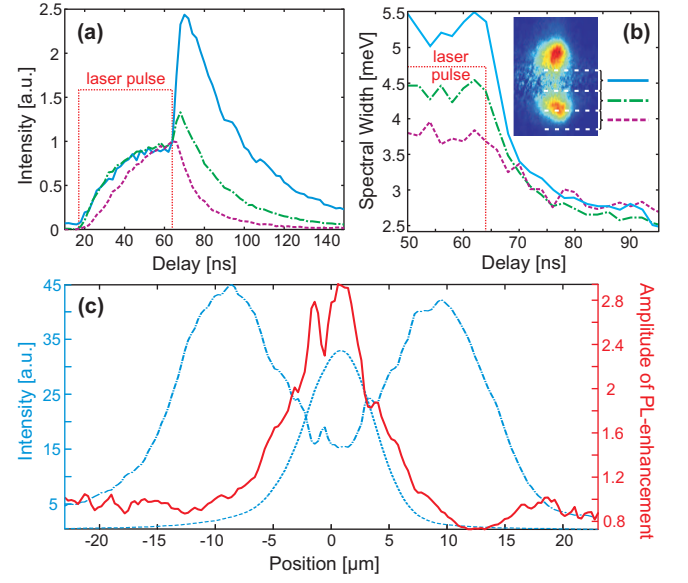


FIG. 4. (Color Online) Normalized time evolution of the maximum of the indirect excitons photoluminescence (a) and the corresponding emission spectral width (b) for $P_{ex} = 14.8 \text{ W.cm}^{-2}$. The blue solid, purple dashed and green dotted-dashed lines correspond to spatial averages of the spectrum at three different positions as shown in the inset displayed in the panel (b). Averaging is done over regions of $7 \mu\text{m}$ width (spatial width of the excitation beam). (c): Spatial profiles of the ring-shaped photoluminescence (dotted-dashed line), excitation beam (dashed line) and PL-enhancement (solid line) for $P_{ex} = 29.6 \text{ W.cm}^{-2}$. The PL-enhancement profile was obtained by dividing the spatial profile 4 ns after the end of pulse (delay 68 ns) by the spatial profile at the end of the pulse (delay 64 ns).

excitons are better thermalized by the semiconductor matrix and the photoluminescence enhancement is absent or reduced. The variation of the spectral linewidth after the laser excitation further supports this interpretation (see Figure 4.b). Indeed, in the central region of the inner-ring the spectral width decreases from 5.2 meV to ~ 3 meV within the first 6 ns that follow the termination of the laser excitation. On the other hand, along the circumference of the inner-ring the spectral width exhibits a decrease reduced to 1 meV in the same time interval. These combined variations indicate that the inner-ring is formed in a regime where the system is dominantly of excitonic type. Indeed, 6 ns after the laser pulse, i.e. in a time interval during which the exciton population has weakly decreased (as shown in Figure 7 indirect excitons exhibit an optical lifetime of ≈ 25 ns), the maximum spectral width lies well below $\Gamma_{e-h}^{(min)}$.

Studying spatially the inner-ring further supports its excitonic origin for our experiments. This is illustrated in Figure 5 where we present the variation of characteristic parameters as a function of the average laser intensity. These are namely the distance between the two local maximum of the emitted inner-ring pattern, r_{ir} , and

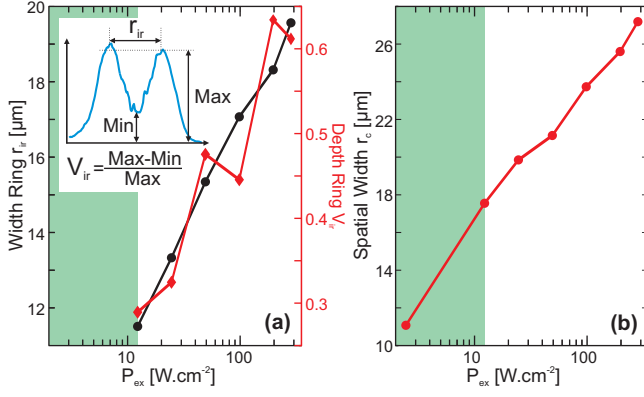


FIG. 5. (Color Online) (a): Characteristics of the ring-shaped photoluminescence for various excitation power at the end of the pulse (delay 64ns). The black line with round markers indicates the width r_{ir} between the two maxima of the spatial profile while the red line with diamond markers indicates the depth V_{ir} of the ring as depicted in the inset. (b): Spatial width 4ns after the end of the pulse (delay 68ns) as a function of the excitation power. In both figures the green shadowed region corresponds to the range of excitation power for which no ring shape can be observed.

the ratio between the maximum and minimum intensities, V_{ir} . In Figure 5.a, we first note that r_{ir} and V_{ir} monotonously increase with the excitation intensity; the variation of V_{ir} is consistent with an increase of the effective temperature of indirect excitons at the position of the laser excitation while outside of the illuminated region excitons have an effective temperature that barely varies. Thus, the laser induced heating results in a temperature gradient that controls the intensity of the emitted photoluminescence and therefore V_{ir} . In addition, the variation of r_{ir} signals that the cloud effective temperature has a spatial profile which is broadened with increasing laser intensity. It also shows that the diffusion of indirect excitons is increased with the exciton concentration, as expected for repulsive dipolar interactions. In that respect, we also show in Figure 5.b the spatial full width at half maximum of the photoluminescence, r_c , i.e. the extension of the exciton cloud. We note as expected that r_c is growing with the laser intensity. Interestingly, r_c increases with a slope that is not modified as we enter the regime where the inner ring is formed. This first indicates that the inner-ring appears in a regime where indirect excitons are effectively delocalized. In addition, it shows that the transport of carriers is not increased in the regime where the inner-ring appears. This observation contrasts with an expected increase of the diffusion at the onset of the Mott transition [9] and then further supports that for our sample the inner-ring manifests the recombination of indirect excitons.

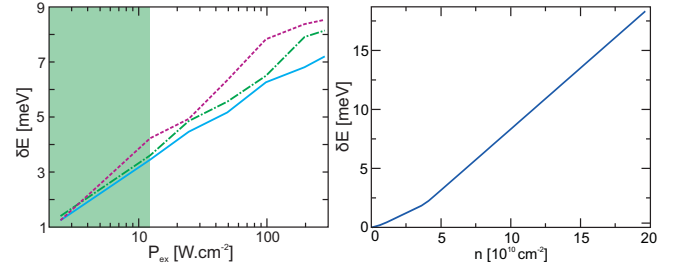


FIG. 6. (Color Online) (a): Blue energy shift of the indirect excitons photoluminescence as a function of the excitation power and measured 4ns after the end of the laser pulse (delay 68ns). The 3 lines correspond to the 3 spatial averages shown in Figure 4. The reference for the shift is the energy position of the indirect exciton line at the lowest excitation power and 100ns after the end of the pulse. (b): Theoretical exciton density as a function of the blue energy shift for a bath temperature of 400 mK.

IV. DISCUSSION

As illustrated in Figure 6.a, for our sample we observed that the photoluminescence signal is largely shifted towards high energies as the laser intensity is increased. We define, the corresponding blue energy shift, δE , as the difference between the spectral position of the photoluminescence emitted at the end of the laser excitation and in the very dilute regime, i.e. following the lowest laser excitation. In Figure 6, we note that the photoluminescence ring is observed for $4 \lesssim \delta E \lesssim 8$ meV which we now relate to the exciton density.

Indirect excitons of DQW constitute well oriented electric dipoles so that repulsive dipole-dipole interactions between excitons induce a shift of the photoluminescence towards higher energies. The resulting energy shift is *a priori* directly related to the exciton density [23], indeed the mean field energy associated to repulsive exciton-exciton interactions scales as $u_0 \cdot n_{2D}$, where n_{2D} is the exciton concentration and u_0 a constant factor controlled by the DQW geometry and the correlations between excitons [24, 25]. In Figure 6.b, we present the exciton concentration that can be deduced from the blue energy shift taking into account the screening of exciton-exciton interactions (see [26] for more details). This approach predicts that the highest exciton density reaches $\approx 10^{11} \text{ cm}^{-2}$ for our experiments which is somewhat very close to the density range at which the Mott transition is expected ($\approx 2 \cdot 10^{11} \text{ cm}^{-2}$). However, we show in the following that in our experiments δE does not reflect directly the density of indirect excitons but rather the role of optically injected carriers that are trapped in the field-effect device.

As mentioned previously, our experiments rely on a laser excitation at an energy greater than the bandgap of the GaAs layers. This results in the injection of free carriers, most of which generate a photocurrent ($\approx 50 \text{ nA}$). A small fraction of optically injected carriers may also

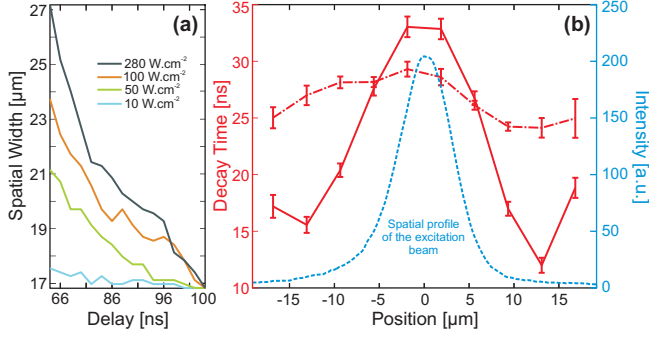


FIG. 7. (Color Online) (a): Time evolution of the spatial width of the photoluminescence emission as a function of the excitation power (the lines organize themselves from bottom to top with increasing excitation power). (b): Spatially resolved decay time for $P_{ex} = 1.8 \text{ W.cm}^{-2}$ (red dotted-dashed line) and $P_{ex} = 29.6 \text{ W.cm}^{-2}$ (red solid line), which are below and above the excitation threshold for the apparition of the inner-ring respectively. Decay times are calculated with a single exponential fit on slice of $3.75 \mu\text{m}$ width (\sim half of the laser spatial width). The spatial profile of the excitation beam is displayed in dashed blue line for sake of comparison.

remain trapped in the device, particularly at the Schottky contact where a potential barrier and gap states are formed [18, 19]. The capture of photo-injected carriers is underlined by the spatial dependence of the photoluminescence energy: while we expect that the photoluminescence is emitted at a higher energy at the position of the laser spot, thus reflecting a higher concentration of indirect excitons, we observe the opposite behavior in Figure 3 with a photoluminescence emitted at an energy which increases with the distance to the center of the laser excitation. This variation for the photoluminescence energy is observed during the laser excitation but also long after (see Fig. 3.e). The dynamics of the exciton cloud after the laser excitation suggests that this behavior is consistent with a trapping of optically injected carriers that increases the amplitude of the electric field towards the laser excited region. Indeed, the photoluminescence decays with a time constant that increases towards the laser spot in the regime where the inner-ring is formed, unlike below the excitation threshold for the formation of the inner-ring (see Fig. 7.b). In addition, Fig. 7.a shows that the spatial extension of the emission rapidly shrinks after the laser pulse, with a characteristic time which decreases as the excitation power increases. These combined observations signal the collection of indirect excitons towards the region that is laser excited and where the electric field is increased: Indirect excitons being high-field seekers, the optical excitation results in the creation of an additional trapping potential. From the spatial emission profile displayed in Figure 3.e-f we estimate that the optically induced trap has a depth of $\sim 1 \text{ meV}$ adding to the box-like trap (with a theoretical 5 meV depth) created by the semitransparent gate electrode.

To confirm experimentally that the large values of δE

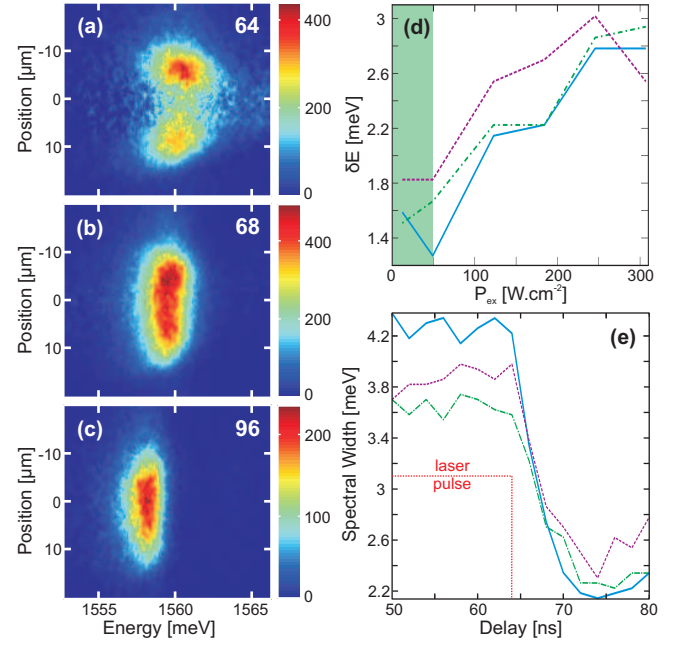


FIG. 8. (Color Online) (a)-(c): Spatially resolved emission spectrum for $P_{ex} = 18.4 \text{ W.cm}^{-2}$ recorded in 2 ns intervals at various time delays for the second field-effect device. The corresponding time delays are indicated on each image. The intensity is colored-scaled independently for each spectrum. (d): Blue energy shift 4 ns after the end of the pulse (68 ns) as a function of the excitation power and for the same 3 spatial averages as the ones shown Figure 4. (e): Time evolution of the spectral width for $P_{ex} = 12.3 \text{ W.cm}^{-2}$ for the same slices mentioned above. Experiments were realized at a bath temperature $T_b = 400 \text{ mK}$

reported previously are due to the trapping of optically injected carriers, we probed a second field-effect device where a super-lattice is placed between the DQW and the top gate electrode. The super-lattice consists of 30 pairs of GaAs/AlAs layers with thickness equal to 3 and 1 nm respectively and positioned 410 nm under the semi-transparent metallic contact. The architecture of the device is otherwise identical to the one shown in Figure 1. The super-lattice is incorporated to confine a fraction of optically injected carriers. Thus, a bi-dimensional plane of charges is formed and can screen the fluctuations of the potential at the top gate electrode which are induced by the laser excitation.

For the second field-effect device, we first confirmed that the inner-ring is formed above an excitation threshold of $\sim 4.9 \text{ W.cm}^{-2}$ which is of the same order of magnitude as for the first sample. However, it exhibits distinct spectroscopic signatures which are summed up in Figure 8. First, we show in Figure 8.d the energy shift of the photoluminescence as a function of the laser intensity under the same experimental conditions as for the experiments shown in Figure 4.b. In general, we note that δE is strongly reduced by the inclusion of the super-lattice, it reaches at most 2.8 meV for the highest laser excita-

tion. This value corresponds to an exciton density of $\sim 5.10^{10} \text{ cm}^{-2}$, i.e. well below the threshold for the Mott transition. Also, during the laser excitation, i.e. when the inner ring is present, we observe that δE decreases with the distance to the laser excitation. This behavior contrasts with the response of our first sample and is consistent with an exciton concentration that decreases with the distance to the laser excitation (see Figure 8.a). Moreover, the spectral width emitted at the center of the inner-ring varies from ~ 4.2 to ~ 2.2 meV between the end of the laser pulse and 10 ns later. On the other hand, it remains narrower along the circumference of the inner-ring and reaches 3.7 meV at the end of the laser pulse and 2.2 meV 10 ns later. Finally, after the laser pulse we note that the photoluminescence is emitted at the same energy all across the exciton cloud (see Fig. 8.b-c). This signals that electric field applied onto the DQW is spatially homogeneous. Indeed, we do not observe any spatial variation of the photoluminescence lifetime unlike for the first device. For the latter, we thus conclude that the internal electric field was varied by optically injected carriers accumulated at the Schottky contact.

V. SUMMARY AND CONCLUSIONS

In summary, we have studied the dynamics of optically created indirect excitons in the regime where the in-

ner photoluminescence ring is formed. Our experiments confirm that at the position of the laser excitation the inner-ring is marked by a sudden increase of the photoluminescence intensity at the end of the laser pulse coincident with a large decrease of the luminescence spectral linewidth. On the other hand, outside of the laser spot the photoluminescence intensity varies weakly after the laser excitation. These observations indicate that the inner-ring is induced by a heating of indirect excitons locally applied by the laser excitation. To further confirm this interpretation, we have studied the exciton density created in our experiments. We have then underlined the role of optically injected carriers which remain trapped at the Schottky contact of the field-effect device where the DQW is embedded. These then vary the internal electric field and accordingly the relation between the blue energy shift of the photoluminescence and the exciton density is blurred. We have then shown that incorporating of a super-lattice between the DQW and the gate electrode efficiently reduces the influence of photo-injected carriers and allowed us to estimate that the exciton concentration is about an order of magnitude lower than the threshold for the Mott transition in the regime where the inner-ring is formed. To conclude, we would like to emphasize that despite its disruptive effect, the trapping of optically injected carriers may provide a new route to realize optically controlled microscopic traps for indirect excitons.

-
- [1] M. Remeika, J. C. Graves, A. T. Hammack, A. D. Meyertholen, M. M. Fogler, L. V. Butov, M. Hanson, and A. C. Gossard, *Phys. Rev. Lett.* **102**, 186803 (2009)
 - [2] M. Alloing, A. Lemaître, F. Dubin, *Europhys. Lett.* **93** 1, 17007 (2011)
 - [3] X. P. Vögele, D. Schuh, W. Wegscheider, J. P. Kotthaus, and A.W. Holleitner, *Phys. Rev. Lett.* **103**, 126402 (2009)
 - [4] A. L. Ivanov, P. B. Littlewood, and H. Haug, *Phys. Rev. B* **59**, 5032 (1999)
 - [5] A. L. Ivanov, *J. Phys.: Condens. Matter* **16**, S3629 (2004)
 - [6] L. V. Butov, A. C. Gossard, D. S. Chemla, *Nature* **418**, 751(2002)
 - [7] D. Snoke, S. Denev, Y. Liu, L. Pfeiffer, K. West, *Nature* **418**, 754 (2002)
 - [8] A. L. Ivanov, L. E. Smallwood, A. T. Hammack, S. Yang, L. V. Butov, A. C. Gossard, *Europhys. Lett.* **73** 6, 920-926 (2006)
 - [9] M. Stern, V. Garmider, E. Segre, M. Rappaport, V. Umansky, Y. Levinson, I. Bar-Joseph, *Phys. Rev. Lett.* **101**, 257402 (2008)
 - [10] A. T. Hammack, L. V. Butov, J. Wilkes, L. Mouchliadis, E. A. Muljarov, A. L. Ivanov, and A. C. Gossard, *Phys. Rev. B* **80**, 155331 (2009)
 - [11] R. Rapaport, G. Chen, D. Snoke, S. H. Simon, L. Pfeiffer, K. West, Y. Liu, S. Denev, *Phys. Rev. Lett.* **92**, 117405 (2004)
 - [12] B. Fluegel, K. Alberi, L. Bhusal, A. Mascarenhas, D. W. Snoke, G. Karunasiri, L. N. Pfeiffer, and K. West, *Phys. Rev. B* **83**, 195320 (2011)
 - [13] A. L. Ivanov, *Europhys. Lett.* **59** 4, 586-591 (2002)
 - [14] A. T. Hammack, N. A. Gippius, Sen Yang, G. O. Andreev, L. V. Butov, M. Hanson, A. C. Gossard, *Jour. of Appl. Phys.* **99**, 066104 (2006)
 - [15] R. Rapaport, G. Chen, S. Simon, O. Mitrofanov, L. Pfeiffer, P. M. Platzman, *Phys. Rev. B* **72**, 075428 (2005)
 - [16] G. Chen, R. Rapaport, L. N. Pfeiffer, K. West, P. M. Platzman, S. Simon, Z. Vörös, D. Snoke, *Phys. Rev. B* **74**, 075428 (2006)
 - [17] A. A. High, A. K. Thomas, G. Grosso, M. Remeika, A. T. Hammack, A. D. Meyertholen, M. M. Fogler, L. V. Butov, M. Hanson, and A. C. Gossard, *Phys. Rev. Lett.* **103**, 087403 (2009)
 - [18] J. Tersoff, *Phys. Rev. Lett.* **52**, 465 (1984)
 - [19] H. Luth, *Solid Surfaces, Interfaces, and Films*, (Springer-Verlag Berlin Heidelberg, New York, NY, (2001))
 - [20] G. J. Schinner, E. Schubert, M. P. Stallhofer, J. P. Kotthaus, D. Schuh, A. K. Rai, D. Reuter, A. D. Wieck, A. O. Govorov, *Phys. Rev. B* **83**, 165308 (2011)
 - [21] The calibration of the excitation power is done considering that 99% of the power is contained in a disk of radius $\sim 1.23 \times$ laser spatial FWHM, the laser beam having a Gaussian profile.
 - [22] We define the amplitude of the PL-jump as the ratio between the maximum of the spectrum detected 4ns after the end of the laser pulse, i.e. at delay 68ns, and at the end of it, i.e. at delay 64ns.

- [23] S. Ben-Tabou de-Leon, B. Laikhtman, Phys. Rev. B **63**, 125306 (2001)
- [24] C. Schindler, R. Zimmermann, Phys. Rev. B **78**, 045313 (2008).
- [25] B. Laikhtman, R. Rapaport, Phys. Rev. B **80**, 195313 (2009).
- [26] A. L. Ivanov, E. A. Muljarov, L. Mouchliadis, and R. Zimmermann, Phys. Rev. Lett. **104**, 179701 (2010)